Directions of seismic anisotropy in laboratory models of mantle plumes

K. A. Druken,[1,2] C. Kincaid,[2] and R. W. Griffiths[3]

Received 23 April 2013; revised 13 June 2013; accepted 14 June 2013; published 19 July 2013.

[1] A recent expansion in global seismic anisotropy data provides important new insights about the style of mantle convection. Interpretations of these geophysical measurements rely on complex relationships between mineral physics, seismology, and mantle dynamics. We report on 3-D laboratory experiments using finite strain markers evolving in time-dependent, viscous flow fields to quantify the range in expected anisotropy patterns within buoyant plumes surfacing in a variety of tectonic settings. A surprising result is that laboratory proxies for the olivine fast axis overwhelmingly align tangential to radial outflow in plumes well before reaching the surface. These remarkably robust, and ancient, anisotropy patterns evolve differently in stagnant, translational, and divergent plate tectonic settings and are essentially orthogonal to patterns typically referenced when prospecting for plume signals in seismic data. Results suggest a fundamental change in the mineral physics-seismology-circulation relationship used in accepting or rejecting a plume model.
Citation: Druken, K. A., C. Kincaid, and R. W. Griffiths (2013), Directions of seismic anisotropy in laboratory models of mantle plumes, *Geophys. Res. Lett.*, *40*, 3544–3549, doi:10.1002/grl.50671.

1. Introduction

[2] Observations of seismic anisotropy, the consequence of the crystallographic or lattice preferred orientation (LPO), can potentially provide powerful constraints on the style of mantle flow that shaped the present-day geology and tectonics of the Earth [e.g., *Russo and Silver*, 1994; *Smith et al*., 2001; *Long and Silver*, 2008], the seismic interpretations of which hinge on a thorough understanding of the relationship between mantle deformation and flow, on the one hand, and the LPO of anisotropic material on the other [e.g., *Savage*, 1999; *Long and Becker*, 2010]. In shear wave splitting studies, the common assumption has been that the seismically fast polarization direction is approximately parallel to the olivine *a* axis [e.g., *Park and Levin*, 2002] and tends to align with the direction of maximum shear [e.g., *Zhang and Karato*, 1995]. However, factors such as dynamic crystallization, water, pressure, and partial melt can potentially complicate this linkage [*Karato et al*., 2008], as well as the time- and spatial-dependent nature of both mantle flow and finite strain [e.g., *McKenzie*, 1979; *Ribe*, 1989; *Buttles and Olson*, 1998; *Kaminski and Ribe*, 2002; *Druken et al*., 2011].

[3] Among the most hotly debated aspects of mantle dynamics is the role, if any, played by buoyant mantle upwellings or hot spot plumes [e.g., *Morgan*, 1972; *Foulger and Natland*, 2003]. At the core of this debate are the expected geological and geophysical surface expressions for mantle plumes [e.g., *Richards et al*., 1989; *Campbell and Griffiths*, 1990; *White and McKenzie*, 1995] and how these relatively small features might appear in seismological [e.g., *Montelli et al.*, 2004; *Behn et al*., 2004; *Farnetani and Samuel*, 2005] and geochemical [e.g., *Schilling*, 1973; *Hofmann and White*, 1982; *Jackson et al*., 2010] data. The simplest, most common view for anisotropy within surfacing plumes is that the fast polarization direction will represent the local buoyant-driven flow, being vertically oriented within the conduit and radially within the pooling, expanding plume head (Figure 1a) [e.g., *Bjarnason et al*., 2002; *Li and Detrick*, 2003; *Xue and Allen*, 2005], which has been supported by LPO calculations within simple models of plume flow [*Blackman et al*., 1996; *Rümpker and Silver*, 2000]. More recent numerical models of LPO within plumes, however, suggest this may not hold entirely true [*Kaminski and Ribe*, 2002; *Fu et al*., 2012].

[4] Here we report results from laboratory fluid dynamics experiments using strain markers designed to reveal the anisotropy pattern in such a spreading plume head and how the pattern is modified by plate-driven flows. Our experimental results reveal the following: (1) axisymmetric plume spreading produces a robust, repeatable axisymmetric pattern in finite strain marker alignments that is orthogonal to the previous expectations; and (2) the shallow tectonic environment can produce spatial and temporal complexity in possible seismic expressions of plumes.

2. Laboratory Methods

[5] Mantle plumes were simulated using glucose syrup with a temperature-dependent density and viscosity in the apparatus of *Druken et al*. [2011]. A volume of syrup was heated in a pressurized reservoir and injected through an insulated 15 mm diameter pipe into an acrylic tank (1 m × 0.6 m × 0.4 m) of glucose at room temperature (Figure 1b). Two motorized spools of transparent Mylar sheeting in contact with the glucose simulated overlying plate motions and provided the desired surface velocities. The less dense (plume) material was injected at the base of the tank and then entered the scaled lower upper mantle region with an average temperature anomaly $\Delta T_{lab} = 4–6°C$ (scaling to $\Delta T_{mantle} \sim 200–300°C$). Length, time, and temperature in the laboratory are related to mantle values using the dimensionless Péclet and Rayleigh numbers (Table 1).

[1]Department of Terrestrial Magnetism, Carnegie Institution of Washington, Washington, D. C., USA.
[2]Graduate School of Oceanography, University of Rhode Island, Narragansett, Rhode Island, USA.
[3]Research School of Earth Sciences, Australian National University, Canberra, ACT, Australia.

Corresponding author: K. A. Druken, Department of Terrestrial Magnetism, Carnegie Institution of Washington, Washington, DC 20015, USA. (kdruken@dtm.ciw.edu)

0094-8276/13/10.1002/grl.50671

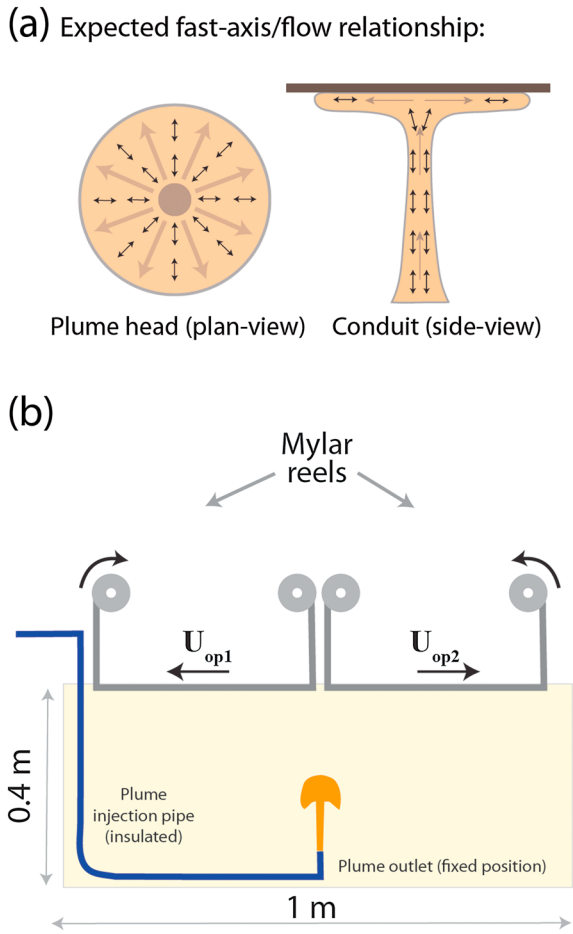

Figure 1. (a) Classic plan and side view expectation of the fast-axis alignment (black lines) within radial plume-driven flow (gray arrows). (b) Cartoon sketch of the laboratory apparatus. Hot buoyant plume material is injected into the tank via an insulated pipe. Two 0.3 m wide Mylar reels (which scale to 1500 km for tectonic plates) are used to generate varied combinations of plate motions. For the sheared case, one reel is utilized, whereas for the stationary surface, both are turned off.

Corresponding laboratory (Earth) scales are approximately 1 mm (5 km), 1 min (5 Ma), and 1°C (50°C), respectively.

[6] Following *Buttles and Olson* [1998], we utilized 5 (±1) mm long synthetic paintbrush hairs, or "whiskers," as passive markers for the evolution of finite strain. Such whiskers have been shown to be a suitable laboratory analog for the motion of the olivine anisotropic fast *a* axis within creep deformation, based upon the continuum theory for LPO by *Ribe* [1989] (refer to *Buttles and Olson* [1998] for a full discussion). The technique provides a relatively simple method for recording high-resolution strain patterns within 3-D time-evolving flow fields. The technique, however, is unable to account for dynamic recrystallization and may not accurately reflect LPO for very small strains [e.g., *Zhang and Karato*, 1995]. But as recent studies on naturally deformed rocks show that larger strains are required for LPO alignment with the shear plane than experimentally deformed samples [e.g., *Warren et al.*, 2008; *Skemer et al.*, 2012], finite strain evolution may still provide a representative approximation for comparison with future models incorporating high-order LPO features (i.e., dynamic recrystallization).

3. Experimental Results

[7] Results are presented for three selected experiments in which the surface forcing is varied to simulate a plume rising from approximately 200 mm (~1000 km) depth beneath the following: (1) a stationary plate, (2) a single migrating plate, and (3) a spreading center (Table 1). In each case, the plume initially forms a classic mushroom-shaped head approximately 60–80 mm in diameter (300–400 km) that subsequently rises at roughly 20 mm/min (~20 mm/yr) before either pooling beneath the surface or experiencing lateral shear due to plate motion.

[8] In the simplest scenario, a plume ascended beneath a stationary surface (a rigid lid imposing a no-slip velocity boundary condition) and the plume remained axisymmetric throughout its evolution (Figure 2a). The ascent rate decreased near the surface, causing the plume head to flatten [e.g., *Griffiths and Campbell*, 1991]. Continued supply of material up the conduit further enhanced radial outflow within the stalled plume head. This is the situation in which the common assumption has been that the seismically fast axis will align vertically within the conduit and radially within the expanding plume head (Figure 1a).

[9] Within the conduit we observe the expected, and coherent, vertical alignment due to the large shear between the near-stationary ambient fluid and vertically ascending plume material (Figure 2a). Within the lateral flow of the plume head, on the other hand, the experiments showed a high degree (~83%) of whisker alignment perpendicular to the flow, in an azimuthal (i.e., circular) pattern (Figures 2b and 2c). Figure 2b shows an illuminated horizontal slice, at 15–30 mm depth, through a plume rising below the stationary surface plate (Experiment 1): despite the purely radial

Table 1. Experimental Parameters for Whisker Alignment Within Plumes[a]

Experiment	ΔT (°C)	U_{op1} (mm min^{-1})	U_{op2} (mm min^{-1})	% Azimuthal Alignment[b]
(1) Stationary surface	4–6	-	-	85
(2) Sheared surface	4–6	40	-	86
(3) Spreading ridge	4–6	30	−30	88

[a]Columns 2–5 represent the approximate laboratory temperature anomaly between ambient and plume material when entering the scaled lower upper mantle region (ΔT), Mylar sheeting rates (U_{op1}, U_{op2}), and the percentage of azimuthal alignment within each plume head. Length, time, and temperature scales are related to the mantle through the Péclet ($Pe = U \times D \kappa^{-1}$) and Rayleigh ($Ra = \rho \times \alpha \times g \times \Delta T \times D^3 \times \kappa \times \mu$) numbers, where U, D, κ, ρ, α, g, and μ represent the surface plate velocity, length scale, thermal diffusivity, density, thermal expansion coefficient, gravitational acceleration, and dynamic viscosity, respectively. For syrup properties, refer to *Kincaid and Griffiths* [2004]. Mantle values of α and ρ are average values from *Turcotte and Schubert* [2002]. Mantle viscosity (μ) was chosen to be an average of upper and lower mantle values (~5×10^{21} Pa s) from *Forte and Mitrovica* [2001]. Resulting laboratory (Earth) scales for length, time, temperature, and velocity became 1 mm (5 km), 1 min (5 Ma), 1°C (50°C), and 1 mm/min (1 mm/yr).

[b]At a distance of ~150 mm from plume source (or 50 mm below surface). Scaled mantle equivalents approximately equal to 750 and 250 km, respectively. Each measurement is an average of all visible whiskers illuminated within the plume head prior to surface plate motion (if applicable).

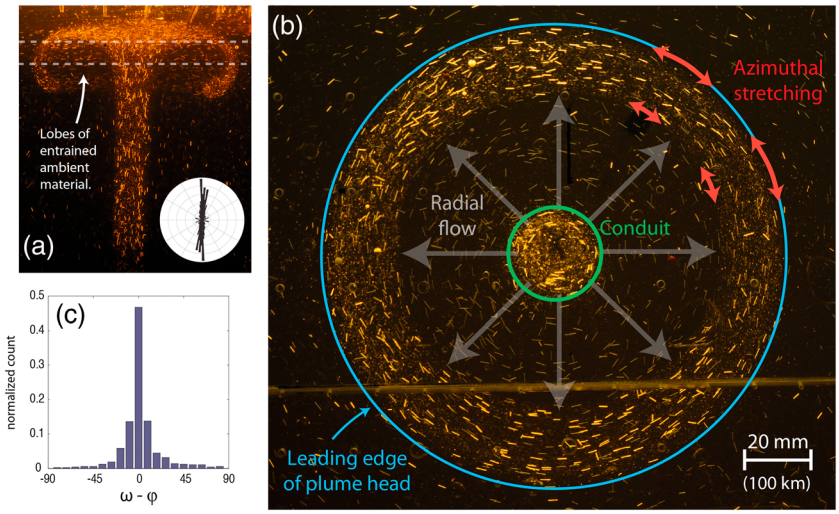

Figure 2. (a) Vertical section (along the axis of symmetry) of the case with no overriding plate motion. All three experiments exhibit substantial whisker alignment (rose diagram inset) with the vertical flow through the conduit. Grey dashed lines highlight the depth of the plan view slice in Figure 2b. (b) Plan view slice 15–30 mm below the surface. Whiskers align normal to the flow as a consequence of azimuthal stretching of the radial outflow in the plume head. Other slices at depths above and below that shown (but within the plume head) display the same azimuthal alignment pattern. (c) Histogram of whisker angles (ω) in Figure 2b relative to the local tangent line. Majority (>83%) of strain markers align within ±15° of the local tangent (i.e., perpendicular to radial flow).

direction of flow everywhere and the strong vertical shear (given the no-slip boundary above and effectively no-slip imposed by the higher viscosity syrup below), there is almost no (< 2%) radial alignment of the whiskers.

[10] This striking azimuthal alignment emerges where the flow leaves the conduit (green circle) and exists through all imaged depths of the plume head, including the sidelobes of the upwelling that contain mostly ambient material entrained during plume-head formation and ascent (Figure 2a). Vertical shear beneath the surface plate works to orient whiskers within the plume head into a horizontal plane as they leave the conduit (just as the horizontal gradient in vertical velocity in the conduit aligns whiskers with the vertical). However, the influence of azimuthal stretching efficiently locks whiskers into a flow-normal, azimuthal orientation (Figure 2c). Specifically, as each material parcel moves through a radius increment, from r to $r+\Delta r$, its azimuthal dimension increases by a fraction $2\pi\Delta r/r$, and its radial dimension is reduced by the same fraction. This represents an extensional pure strain in the horizontal plane.

[11] Early-stage whisker patterns in cases with surface motion (Experiments 2 and 3) are again marked by vertical alignment within the conduits and azimuthal alignment within the plume heads (Figures 3a and 3d), consistent with the case of no plate motion (Figure 2, Experiment 1). As time evolves, whiskers show a range of finite strain patterns that include flow-normal and flow-parallel alignments, as well as regions having little or no coherent pattern. When rising beneath a single migrating plate, the tilted plume head exhibits predominantly flow-normal orientations that weak plate-driven shear in the horizontal plane is unable to erase (Figure 3b, Experiment 2, dashed gray box). There is also strong apparent alignment along the sides of this tilted feature (Figure 3b, magenta dashed boxes), which only coincidentally reflects the direction of flow as a result of the azimuthal alignment in the earlier radial spreading phase (Figure 3a). The remaining central core of the tilted plume feature displays no strong relationship between whisker orientation and flow direction (≲55%), despite the simple plate motion (Figure 4a). This area of weak alignment represents the tilting of the conduit from a vertical to subhorizontal orientation beneath the moving plate (Figure 3c).

[12] Diverging plates at a mid-ocean ridge produce an environment of greater strain, and the rising plume is essentially cloven in two as the material is drawn out evenly beneath the two plates (Figure 3e). The larger strain produces a bimodal distribution of whisker alignments and a simpler connection with the local plate-driven flow field (Figures 3e and 3f). In one region of the flow, a coherent flow-normal alignment results from the lateral displacement of half the stalled plume head by plate stress (Figure 3e, gray dashed boxes): the pattern in this zone is again historic, having formed prior to arrival at the surface. The plume head does not remain within the extensional area long enough for whisker orientations to be altered and remains roughly flow-normal over the entire course of the experiment (~100 Ma). The second observed pattern is associated with a thin (~10 mm) and narrow (~20 mm wide) strip beneath each plate (Figures 3e and 3f, magenta dashed boxes) and shows the vertical alignment from the conduit rotated into a subhorizontal, flow-parallel direction by the extensional stresses beneath the spreading center. The alignment becomes more complete (>80% alignment with flow direction) with time (Figure 4a) as extension continues, and the plume head has been carried a (scaled) distance greater than 1300 km distance from the ridge (Figure 3f).

4. Discussion

4.1. Deformation History

[13] A robust feature of these experiments is the repeatable nature of the azimuthal pattern, which, once developed, is difficult to disturb or realign. In the present experiments, the azimuthal whisker orientations are initialized during the deep

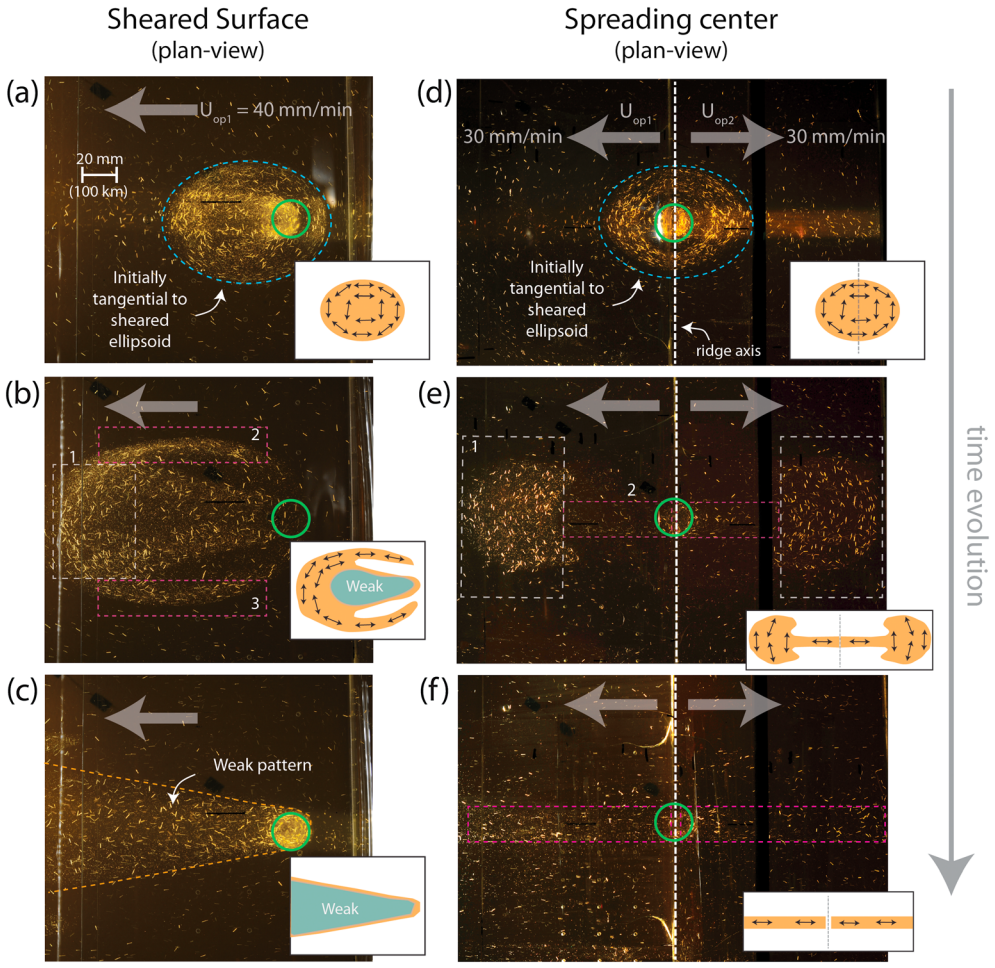

Figure 3. Time evolution of plumes beneath a sheared surface simulating (a–c) a moving tectonic plate and (d–f) divergent spreading center. Blue dashed ellipsoids outline the initial shape of the plume head prior the start of plate motions, and gray arrows illustrate plate velocities. Gray and magenta dashed boxes highlight regions of plate flow-normal and flow-parallel alignment, respectively, and insets display a simplified cartoon sketch of the average patterns observed. In the case of the plume sheared by overriding plate motion, the outer perimeter displays strong alignment patterns, whereas only a weak alignment is found in the area closest to the conduit. For the plume rising beneath a spreading center, a combination of shearing of the plume head normal to the ridge and extension of the plume along the ridge results in strong whisker alignments in areas of flow-normal alignment and areas of flow-parallel alignment.

formation of the plume head long before interaction with the surface (Figure 4b). More than 65% of markers in each case have this distinct alignment within a scaled distance of 100–200 km from the source, which then strengthens (>85%) as conduit material continues to feed the plume head over the ~1000 km (scaled) distance to the surface. Preexisting, or historical, whisker conditions are then inherited from below, as demonstrated by the case of a plume reaching the surface beneath a single, laterally moving plate (Figures 3a–3c) or beneath a spreading center (Figures 3d–3f). Surface shear in both cases is unable to erase this historic pattern over the timescales of each experiment (~100 Ma), suggesting that the deformation history [e.g., *Warren et al.*, 2008; *Skemer et al.*, 2012] may play an important role in shallow LPO alignment within plumes.

4.2. Comparison With Previous Models of Plume Flow and LPO

[14] A discrepancy between our laboratory observations and the earliest numerical simulations of LPO alignment within similar flow systems [*Blackman et al.*, 1996; *Rümpker and Silver*, 2000] arises from model constraints. Both numerical studies generated either purely two-dimensional or axisymmetric model solutions from a two-dimensional domain rotated about a vertical axis. While these may be appropriate for simple models of plume flow, the evolution of the olivine *a* axis was constrained by the planar solution and forced into a radial or flow-parallel alignment. Deformation and resulting *a* axis orientations in two-dimensional calculations are unable to reflect a time-evolving three-dimensional flow field, which includes the azimuthal extension and deformation history that are the essential elements in strain and whisker alignment. Our results are, however, in agreement with recent three-dimensional numerical models of shallow plume dispersion [*Fu et al.*, 2012], which observe flow-perpendicular alignment within similar depths of expanding plume material. For sheared conduit regions (Figure 3c, Experiment 2), the variable whisker pattern is also consistent with the weakly flow-aligned LPO calculated by *Kaminski and Ribe* [2002] in their model of a sheared buoyant cylinder nearby a ridge.

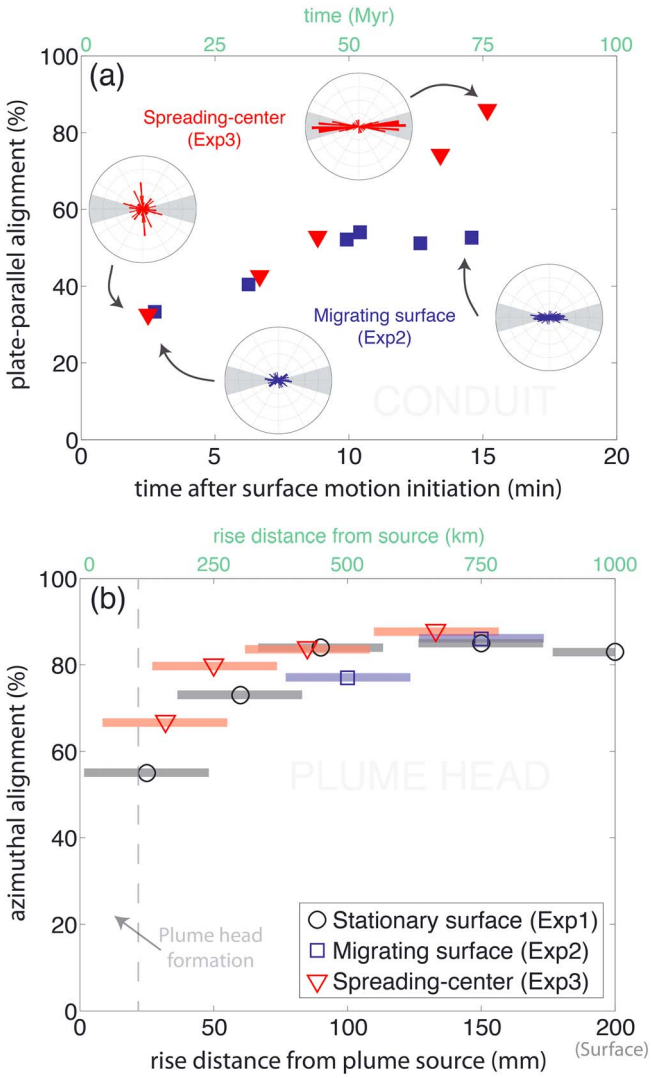

Figure 4. (a) Plate-parallel alignment percentage ($0° \pm 15°$) versus time within the conduit region(s) for those experiments with a migrating surface ($t = 0$ being the initiation of plate motion). Measurements were calculated for conduit whiskers located within 150 mm (750 km) radius of the source position. Rose diagram insets illustrate the range of whisker orientations at the beginning and end of each experiment (the outer rim of each angle histogram represents ~15% of the total whisker count). (b) The percent azimuthal alignment averaged over the entire plume head as a function of rise distance from the plume source, prior to any disruption from surface motion (shaded bars represent the depths each measurement was averaged over). Plumes develop a deep azimuthal pattern (>55% alignment) immediately following plume head formation that is then carried to the shallow subplate environment.

4.3. Implication for Seismic Anisotropy Observations

[15] Assuming an olivine LPO where the fast axis is expected to align roughly parallel to the maximum direction of shear or extension (e.g., A-type fabric), the experimental results are consistent with vertically oriented LPO within plume conduits but inconsistent with radial patterns within plume heads. The results instead imply that radial flow within plume heads as they approach the surface will display flow-perpendicular or azimuthally aligned fabrics. With surface plate motion, however, the connection between finite strain alignment and flow becomes more spatially and temporally complex, particularly as sheared conduit material begins to reach the surface (Figure 3). The roughly flow-perpendicular pattern from the plume head dominates the smaller-volume material from the conduit, leading to incoherent alignment patterns during the early stages (≲30 Ma) of each experiment (Figure 4a).

[16] For the specific case of a plume rising beneath a single moving lithospheric plate (Experiment 2), the weak flow-parallel alignment (< 55%) in the conduit region persists throughout the entire experiment and may explain the often large variation in regional shear wave splitting observations at hot spot locations, despite the relatively simple plate motions [e.g., *Waite et al.*, 2005; *Walker et al.*, 2005; *Collins et al.*, 2012]. The results for a plume rising at a spreading center imply that the combination of ridge-normal and ridge-parallel alignment of the olivine fast axis detected at the Iceland plume-ridge interaction [*Bjarnason et al.*, 2002; *Li and Detrick*, 2003; *Xue and Allen*, 2005] may be explained by past variation of flow deformation zones, possibly in conjunction with localized flow. But as anisotropy observations are typically a path-integrated value, the sheared plume layer may volumetrically begin to contribute little to the total sampled anisotropic layer at mature hot spot locations, where the plume head has long been advected away. This would be supported by the relatively good agreement between fast polarization directions at ocean island stations and global models that incorporate plate and density-driven flow [e.g., *Behn et al.*, 2004].

5. Conclusions

[17] Despite many complicating factors in the interpretation of seismic anisotropy in terms of mantle flow, the laboratory experiments provide insight to the styles of deformation (pure versus simple shear) to be expected in the case of mantle plumes in various tectonic settings. The flow deformation and alignment patterns identified in these cases will hopefully serve as new models for future interpretations of seismic data. The results highlight the following: (1) azimuthal stretching of flow within plume heads, which produces highly coherent alignment in a azimuthal pattern; (2) the difficulty of mapping complex three-dimensional and time-varying conduit regions; and (3) a significant role played by the flow history during the ascent of plumes in producing the azimuthal or flow-normal alignment pattern. While future modeling to investigate the role of varied plume buoyancy and plate rates is needed, these observations may prove important for future calculations of LPO within flow models and for inferences about mantle flow drawn from seismic anisotropy.

[18] **Acknowledgments.** Experiments were conducted at the GFD Laboratory at the Research School of Earth Sciences, Australian National University. We thank Tony Beasley for his expert technical assistance and help with the discovery of these whisker patterns. We also thank Kial Stewart, Alex Song, and Garrett Ito for helpful discussion and two anonymous reviewers who helped improve this manuscript. This work was supported by NSF grants EAR-0652512/EAR-0506857 and a Carnegie DTM Postdoctoral Fellowship (KAD).

[19] The Editor thanks James Conder and Mark Behn for their assistance in evaluating this paper.

References

Behn, M. D., C. P. Conrad, and P. G. Silver (2004), Detection of upper mantle flow associated with the African Superplume, *Earth Planet. Sci. Lett.*, *224*, 259–274.

Bjarnason, I. T., P. G. Silver, G. Rümpker, and S. C. Solomon (2002), Shear wave splitting across the Iceland hot spot: Results from the ICEMELT experiment, *J. Geophys. Res.*, *107*(B12), 2382, doi:10.1029/2001JB000916.

Blackman, D. K., J. M. Kendall, P. R. Dawson, H. R. Wenk, D. Boyce, and J. P. Morgan (1996), Teleseismic imaging of subaxial flow at mid-ocean ridges: Traveltime effects of anisotropic mineral texture in the mantle, *Geophys. J. Int.*, *127*, 415–426.

Buttles, J., and P. Olson (1998), A laboratory model of subduction zone anisotropy, *Earth Planet. Sci. Lett.*, *164*, 245–262.

Campbell, I. H., and R. W. Griffiths (1990), Implications of mantle plume structure for the evolution of flood basalts, *Earth Planet. Sci. Lett.*, *99*, 79–93.

Collins, J. A., C. J. Wolfe, and G. Laske (2012), Shear wave splitting at the Hawaiian hot spot from the PLUME land and ocean bottom seismometer deployments, *Geochem. Geophys. Geosyst.*, *13*, Q02007, doi:10.1029/2011GC003881.

Druken, K. A., M. D. Long, and C. R. Kincaid (2011), Patterns in seismic anisotropy driven by rollback subduction beneath the High Lava Plains, *Geophys. Res. Lett.*, *38*, L13310, doi:10.1029/2011GL047541.

Farnetani, C. G., and H. Samuel (2005), Beyond the thermal plume paradigm, *Geophys. Res. Lett.*, *32*, L07311, doi:10.1029/2005GL022360.

Forte, A. M., and J. X. Mitrovica (2001), Deep-mantle high-viscosity flow and thermochemical structure inferred from seismic and geodynamic data, *Nature*, *410*, 1049–1056.

Foulger, G. R., and J. H. Natland (2003), Is "hotspot" volcanism a consequence of plate tectonics?, *Science*, *300*, 921–922.

Fu, Y. V., L. Aibing, and S. Hung (2012), Waveform modeling of shear wave splitting from anisotropic models in Iceland, *Geochem. Geophys. Geosyst.*, *13*, Q12001, doi:10.1029/2012GC004369.

Griffiths, R. W., and I. H. Campbell (1991), The interaction of plumes with the Earth's surface and onset of small-scale convection, *J. Geophys. Res.*, *96*, 18,295–18,310.

Hofmann, A. W., and W. M. White (1982), Mantle plumes from ancient oceanic crust, *Earth Planet. Sci. Lett.*, *57*, 421–436.

Jackson, M., S. R. Hart, J. G. Konter, A. A. P. Koppers, H. Staudigel, M. D. Kurz, J. Blusztajn, and J. M. Sinton (2010), Samoan hot spot track on a "hot spot highway": Implications for mantle plumes and a deep Samoan mantle source, *Geochem. Geophys. Geosyst.*, *11*, Q12009, doi:10.1029/2010GC003232.

Kaminski, É., and N. M. Ribe (2002), Timescales for the evolution of seismic anisotropy in mantle flow, *Geochem. Geophys. Geosyst.*, *3*(8), 1051, doi:10.1029/2001GC000222.

Karato, S., H. Jung, I. Katayama, and P. Skemer (2008), Geodynamic significance of seismic anisotropy of the upper mantle: New insights from laboratory studies, *Annu. Rev. Earth Planet. Sci.*, *36*, 59–95.

Kincaid, C., and R. W. Griffiths (2004), Variability in flow and temperature within mantle subduction zones, *Geochem. Geophys. Geosyst.*, *5*, Q06002, doi:10.1029/2003GC000666.

Li, A., and R. S. Detrick (2003), Azimuthal anisotropy and phase velocity beneath Iceland: Implication for plume-ridge interaction, *Earth Planet. Sci. Lett.*, *214*, 153–165.

Long, M. D., and T. W. Becker (2010), Mantle dynamics and seismic anisotropy, *Earth Planet. Sci. Lett.*, *297*, 341–354.

Long, M. D., and P. G. Silver (2008), The subduction zone flow field from seismic anisotropy: A global view, *Science*, *319*, 315–318.

McKenzie, D. (1979), Finite deformation during fluid flow, *Geophys. J. R. Astron. Soc.*, *58*, 689–715.

Montelli, R., G. Nolet, F. A. Dahlen, G. Masters, E. R. Engdahl, and S. Hung (2004), Finite-frequency tomography reveals a variety of plumes in the mantle, *Science*, *303*, 338–343, doi:10.1126/science.1092485.

Morgan, W. J. (1972), Plate motions and deep convection, *Mem. Geol. Soc. Am.*, *132*, 7–22.

Park, J., and V. Levin (2002), Seismic anisotropy: Tracking plate dynamics in the mantle, *Science*, *296*, 485–489.

Ribe, N. M. (1989), Seismic anisotropy and mantle flow, *J. Geophys. Res.*, *94*, 4213–4223.

Richards, M. A., R. A. Duncan, and V. E. Courtillot (1989), Flood basalts and hot-spot tracks: Plume heads and tails, *Science*, *246*, 103–107.

Rümpker, G., and P. G. Silver (2000), Calculating splitting parameters for plume-type anisotropic structures of the upper mantle, *Geophys. J. Int.*, *143*, 507–520.

Russo, R. M., and P. G. Silver (1994), Trench-parallel flow beneath the Nazca Plate from seismic anisotropy, *Science*, *263*, 1105–1111.

Savage, M. K. (1999), Seismic anisotropy and mantle deformation: What have we learned from shear wave splitting?, *Rev. Geophys.*, *37*, 65–106.

Schilling, J. G. (1973), Iceland Mantle plume: Geochemical study of Reykjanes Ridge, *Nature*, *242*, 565–571.

Skemer, P., J. M. Warren, and G. Hirth (2012), The influence of deformation history on the interpretation of seismic anisotropy, *Geochem. Geophys. Geosyst.*, *13*, Q03006, doi:10.1029/2011GC003988.

Smith, G. P., D. A. Wiens, K. M. Fischer, L. M. Dorman, S. C. Webb, and J. A. Hildebrand (2001), A complex pattern of mantle flow in the Lau Backarc, *Science*, *292*, 713–716.

Turcotte, D. L., and G. Schubert (2002), *Geodynamics*, 2nd ed., Cambridge Univ. Press, Cambridge, U. K.

Waite, G. P., D. L. Schutt, and R. B. Smith (2005), Models of lithosphere and asthenosphere anisotropic structure of the Yellowstone hot spot from shear wave splitting, *J. Geophys. Res.*, *110*, B11304, doi:10.1029/2004/JB003501.

Walker, K. T., G. H. R. Bokelmann, S. L. Klemperer, and G. Bock (2005), Shear-wave splitting around the Eifel hotspot: Evidence for a mantle upwelling, *Geophys. J. Int.*, *163*, 962–980.

Warren, J. M., G. Hirth, and P. B. Kelemen (2008), Evolution of olivine lattice preferred orientation during simple shear in the mantle, *Earth Planet. Sci. Lett.*, *272*, 501–512.

White, R. S., and D. McKenzie (1995), Mantle plumes and flood basalts, *J. Geophys. Res.*, *100*, 17,543–17,585.

Xue, M., and R. M. Allen (2005), Asthenospheric channeling of the Icelandic upwelling: Evidence from seismic anisotropy, *Earth Planet. Sci. Lett.*, *235*, 167–182.

Zhang, S., and S. Karato (1995), Lattice preferred orientation of olivine aggregates deformed in simple shear, *Nature*, *375*, 774–777.